European Journal of Radiology 116 (2019) 152–159

Contents lists available at ScienceDirect

European Journal of Radiology

journal homepage: www.elsevier.com/locate/ejrad

Research article

Isolated periventricular pseudocysts do not affect white matter microstructure development in neonatal stage: A retrospective case-control diffusion tensor imaging study

Miaomiao Wang[a], Congcong Liu[a], Xianjun Li[a], Heng Liu[a,b], Chao Jin[a], Xingxing Tao[a], Xiaoyu Wang[a], Huifang Zhao[a], Yannan Cheng[a], Fan Wu[a], Yuli Zhang[a], Jian Yang[a,b,*]

[a] Department of Diagnostic Radiology, the First Affiliated Hospital of Xi'an Jiaotong University, Xi'an, 710061, PR China
[b] Department of Biomedical Engineering, School of Life Science and Technology, Xi'an Jiaotong University, Xi'an, 710054, PR China

ARTICLE INFO

Keywords:
Periventricular pseudocysts
Neonates
Diffusion tensor imaging
White matter development

ABSTRACT

Background and Purpose: Periventricular pseudocysts (PVPCs) are cystic cavities originating from the germinal matrix. The effects of PVPCs on the development of white matter (WM) in neonates remain unclear. This study aimed to characterise WM microstructural variations in neonates with PVPCs with and without additional abnormities on MRI.

Materials and methods: Neonates with PVPCs and controls with no MRI abnormalities were retrospectively enrolled. Test subjects were divided into groups 1 (isolated PVPCs) and 2 (PVPCs with additional MRI abnormalities). The PVPC MRI features collected included lateralisation, locularity, anatomic location, and the maximum anteroposterior diameter. Diffusion tensor imaging (DTI)-derived fractional anisotropy (FA), radial diffusivity (RD), and axial diffusivity (AD) were compared between the PVPC and control groups using tract-based spatial statistics.

Results: Thirty-eight neonates with PVPCs and 60 controls were enrolled. Groups 1 and 2 contained 15 and 23 subjects, respectively. The additional MRI findings in group 2 included intracranial haemorrhage, punctate WM lesions, hypoxic-ischaemic encephalopathy, and acute cerebral infarction. No significant differences were found in PVPC MRI features between the 2 test groups. Compared to controls, no significant changes in DTI metrics were observed in group 1 neonates; whereas extensive WM regions with decreased FA, increased RD, and unchanged/increased AD were found in group 2.

Conclusions: Isolated PVPCs are not independently correlated with WM microstructural variations in neonates. This result provides further evidence for supporting the benign outcome of fetuses with isolated PVPCs.

1. Introduction

Periventricular pseudocysts (PVPCs) are cystic cavities that lack the true ependymal cell lining and are surrounded by germinal cells and glial tissue [1,2]. PVPCs are identified in an estimated 0.5–5.8% of neonates by cranial ultrasound (US) examination [1,3,4]. However, the insensitivity of cranial US to white matter (WM) has caused long-standing confusion between PVPCs and cystic periventricular leukomalacia, which has a poor prognosis [5]. The presence of PVPCs was believed to be significantly associated with abnormal neurodevelopment (leading to muscle tone abnormalities, cerebral palsy, developmental delay, attention deficit hyperactivity and autistic spectrum disorder) [6–9]. The pathogenetic mechanisms of PVPC formation proposed to date include haemorrhage and germinolysis in the germinal matrix [3,4,10]. Because the germinal matrix generates neural stem cells, which in turn give rise to neurons, astrocytes, and oligodendrocytes [11], it remains unclear whether PVPCs alone can affect WM development. MRI based on morphology- and tissue-microstructure-dependent contrast can precisely detect small cysts and their locations and is therefore superior to US for assessment of brain

Abbreviations: PVPCs, periventricular pseudocysts; WM, white matter; DTI, diffusion tensor imaging; FA, fractional anisotropy; RD, radial diffusivity; AD, axial diffusivity; US, ultrasound; TBSS, tract-based spatial statistics; GA, gestational age; SWI, susceptibility-weighted imaging; T1WI, T1-weighted imaging; T2WI, T2-weighted imaging; TR, repetition time; TE, echo time; FOV, field of view; CTN, caudothalamic notch; HIE, hypoxic-ischaemic encephalopathy; TORCH, toxoplasmosis rubella, cytomegalovirus, and herpes simplex virus

* Corresponding author at: Department of Diagnostic Radiology, The first Affiliated Hospital of Xi'an Jiaotong University, Xi'an, 710061, PR China.
E-mail address: yj1118@mail.xjtu.edu.cn (J. Yang).

https://doi.org/10.1016/j.ejrad.2019.05.005
Received 18 January 2019; Received in revised form 17 April 2019; Accepted 5 May 2019

development and injury, especially in the WM region [4,10]. Since neonatal WM microstructural features are closely associated with developmental outcomes [12], early assessment of the relationship between PVPCs and WM development is of great significance to parental decision-making and obstetric management.

Diffusion tensor imaging (DTI) provides quantitative metrics derived from fibre coherence, axonal density, and myelination, and is consequently more sensitive and objective for assessment of brain maturation and detection of WM injury than conventional MRI sequences [13]. Fractional anisotropy (FA), axial diffusivity (AD) and radial diffusivity (RD) are three DTI based parameters used to quantify the integrity of WM microstructure by measuring the degree of anisotropy, the magnitude of water diffusion along and perpendicular to the axons. With brain development, FA increases are accompanied by a decrease in AD and RD in all WM regions [12]. Tract-based spatial statistics (TBSS; http://fsl.fmrib.ox.ac.uk/fsl/fslwiki/TBSS) is an automated, observer-independent approach to assessing differences in DTI parameters on major WM tracts [14]. Further characterisation of alterations in the WM has been proposed using region of interest (ROI) analysis [15]. These automated quantitative DTI data processing methods have all been used to detect abnormalities due to brain development or injury [16,17], and are promising tools for characterisation of the alterations associated with PVPCs.

The goal of this study was to characterise the extent of WM microstructural variations in PVPC neonates with and without additional MRI abnormities, using DTI combined with TBSS and ROI analysis.

2. Materials and methods

This retrospective study was conducted with approval from the relevant institutional review board. The parents of all neonates were informed of the risks of MR imaging and provided written consent.

2.1. Subjects

Neonates who underwent MRI examination at the Department of Diagnostic Radiology of a local hospital from August 2013 to October 2017 were enrolled in this retrospective case-control study.

Neonates in the PVPC groups were eligible for inclusion if they met the following conditions: (1) gestational age (GA) $<$ 42 weeks; (2) age at MRI $\leq$ 28 days; and (3) evidence of a PVPC on conventional MRI. Exclusion criteria were as follows: (1) pachygyria (abnormally thick cortex with reduced formation of the cerebral convolutions); (2) incomplete DTI images or clinical information (including perinatal characteristics and clinical condition). Neonates with PVPCs were classified into 2 groups. Group 1 (isolated PVPCs) included cases with PVPCs as the only findings on MRI. Group 2 (PVPCs with additional abnormalities) included cases of PVPCs with any additional abnormalities on routine MRI examination. Neonates in the control group underwent brain MRI examinations for screening brain injury were enrolled in accordance with the following criteria: (1) GA $<$ 42 weeks; (2) age at MRI $\leq$ 28 days; and (3) no abnormalities on routine MRI examination (for suspected cases of haemorrhage and vascular malformation, supplementary identification of these disorders using susceptibility weighted imaging [SWI] was used to eliminate uncertainty). Neonates with incomplete clinical information were excluded from the selection process for the control group.

The peri- and neonatal variables of all subjects were collected from the medical records. These included perinatal history, clinical conditions, and PVPC MRI features.

2.2. MRI acquisition

MRI data were acquired using a 3.0-T scanner (Signa HDxt, GE, WI, USA) with an 8-channel head coil. To reduce motion artefacts and increase the MRI completion rate, all neonates had their sleep and feeding protocols adjusted; those unable to remain still were sedated with a relatively low dose of 10% chloral hydrate (25–50 mg/kg body weight) with the guardians' approval [18]. The potential risks of chloral hydrate were fully considered [19], and the neonates were monitored for adverse drug reactions for 24 h. Micro-earplugs were used to protect the neonates' hearing. The subjects' heads were immobilised by moulded foam placed around the head.

Three-dimensional fast spoiled gradient-recalled echo T1 weighted imaging (T1WI), fast spin-echo T2 weighted imaging (T2WI), single-shot echo-planar DTI, and SWI were performed. The scanning parameters of each sequence were as follows: (1) three-dimensional fast spoiled gradient-recalled echo T1WI: repetition time (TR)/echo time (TE) = 10.18/4.62 ms, slice thickness = 1 mm with no gap; field of view (FOV) = 240 mm; and matrix size = 256 × 256; (2) fast spin-echo T2WI: TR/TE = 4200/118.9 ms; slice thickness = 4 mm with no gap; FOV = 180 mm; and matrix size = 192 × 192; (3) DTI: 30 gradient directions; the number of excitations = 1; b values = 0 and 600 s/mm^2; TR/TE = 11000/69.5 ms; slice thickness = 2.5 mm with no gap; FOV = 180 × 180 mm; and matrix size = 128 × 128; (4) SWI: TR/TE = 51/6–60 ms; slice thickness = 2 mm with no gap; FOV = 180 mm; and matrix size = 384 × 256. The total scan time was approximate 30 minutes

2.3. MRI features

PVPCs were defined according to the study by Epelman et al. [20] and were usually located at the external angle of the lateral ventricles or on the floor close to the caudothalamic groove. Two experienced radiologists (9 and 5 years of experience in the interpretation of neonatal brain MR images, respectively), blinded to the clinical history of the neonates, independently analysed the MRI data. The following PVPC features were recorded: lateralization (bilateral/left/right side); locularity (uni-/multi-); and anatomic location in relation to the ventricle horns (frontal/temporal/occipital horns and proximity to the caudothalamic notch [CTN]/adjacent to the head of caudate nucleus) [3]. The maximum anteroposterior diameter of the PVPC was evaluated on axial T1WI images. Other MRI abnormalities were also evaluated. Disagreements regarding imaging findings were resolved by discussion and mutual agreement.

2.4. Data analysis

2.4.1. Processing of DTI data

DTI data were processed using the FMRIB software library (FSL, http://www.fmrib.ox.au.uk/fsl) [21]. Eddy current correction and brain region extraction were performed. To ensure the adequate image quality for further analysis, we rejected artifact-corrupted directions automatically before tensor estimation [22]. The number of rejected directions varied across subjects (median = 5; range, 0–17). The DTI metrics of FA, AD, and RD were calculated using the FMRIB Diffusion Toolbox (http://fsl.fmrib.ox.ac.uk/fsl/fslwiki/FDT).

2.4.2. Voxelwise analysis of TBSS

Image registration was performed using an optimised protocol including the following 5 steps [14]. (1) To obtain the general characteristics of the group, the first group mean FA image in a native space was created using data of the study subjects. (2) The images of all subjects were linearly registered (6 and 12 degrees of freedom) to the first group mean image, and the second group mean FA image was obtained. (3) After all individual images had been registered to the second group mean FA image using a combination of linear and nonlinear methods, the single-subject FA image with the lowest mean displacement score in control group was selected as the final target. (4) All individual FA images were registered to the target using the same registration process. (5) Other metrics were normalised to the target space using the FA deformation parameters.

The normalised individual FA images were up-sampled to a voxel size of 1 × 1 × 1 mm and then were averaged to create the mean FA. A mean FA skeleton was extracted from the mean FA to represent the centre of WM tracts. The threshold of the FA skeleton was 0.15. DTI metrics were projected onto this skeleton prior to statistical analysis.

2.4.3. ROI analysis

Brain regions with differences in DTI parameters between neonates with PVPCs and controls were extracted for further investigation by ROI analysis. To ensure standardisation, ROIs of each hemisphere were selected for comparison according to the JHU neonatal brain atlas [23].

2.4.4. Statistical analysis

Wilcoxon signed-rank tests were used to assess between-group differences in demographics (GA, age at MRI, birth weight, head circumference, and body length), which were not normally distributed. Inter-group differences in sex, mode of delivery, clinical condition, and PVPC MRI features were evaluated using chi-square and Wilcoxon signed-rank tests. All statistical analyses were performed using SPSS 19.0 (SPSS, Inc., Chicago, IL, USA). Differences of $P < 0.05$ between the two PVPC groups were considered to be statistically significant; in multiple comparisons, $P < 0.017$ (0.05/3) was considered statistically significant after the Bonferroni correction.

The FSL Randomize tool (http://fsl.fmrib.ox.ac.uk/fsl/fslwiki/Randomise/UserGuide) was used for voxel-wise analysis to compare the PVPC and control groups. The number of permutations was 10,000. Tests in TBSS were considered significant at $P < 0.017$ (0.05/3) after the threshold-free cluster enhancement and family-wise error rate correction. The DTI-derived values of brain regions with significant differences in neonates with PVPC were further compared with those of controls by Wilcoxon signed-rank tests.

3. Results

3.1. Demographics

Brain MRI examinations of 323 consecutive neonates were evaluated retrospectively, and 46 (14.24%) neonates with PVPCs and 79 controls fulfilled the inclusion criteria. Eight neonates with PVPCs were excluded because of incomplete DTI images (n = 6), incomplete clinical information (n = 1), and pachygyria malformations (n = 1). In the control group, 19 neonates were excluded because of incomplete clinical information. Eventually, 38 neonates with PVPCs and 60 controls were enrolled. Fifteen and 23 neonates with PVPCs were classified into groups 1 and 2, respectively, based on their MRI findings (Fig. 1). Groups 1 and 2 were compared with the control group, and no significant differences in demographic data were found (Table 1). The clinical conditions of the subjects are summarised in Table 1. The incidence of clinical infection alone ($P_{group1} = 0.01$, $P_{group2} < 0.001$) was significantly higher in the 2 PVPC groups than in the control group. The incidences of the other recorded comorbid clinical conditions were not significantly different between the PVPC and control groups ($P > 0.017$, details in Table 1).

3.2. PVPC imaging findings

The PVPC imaging characteristics are summarised in Table 2. Of the 38 PVPCs detected, 21(55.26%), 12 (31.58%) and 5 (13.16%) were separately located on the bilateral, left and right side. Most of the PVPCs (34/38, 89.47%) were unilocular. In 33 cases (86.84%), the PVPCs were extended to the CTN/adjacent to the head of the caudate nucleus. In 5 cases (13.16%), the PVPCs were located along the frontal horns, while in only 1 case (2.63%), the pseudocyst was located along the occipital horns. No significant differences in lateralisation, locularity, location, or maximum anteroposterior diameter were observed between the 2 PVPC groups.

The additional MRI findings of the 23 neonates with PVPCs in group 2 including extracerebral haemorrhage (n = 5), parenchymal haemorrhage (n = 2), parenchymal and extracerebral haemorrhage (n = 2), extracerebral and intraventricular haemorrhage (n = 1), mild to severe punctate WM lesions (n = 7), mild to moderate punctate WM lesions combined with extracerebral haemorrhage (n = 2), moderate punctate WM lesions combined with parenchymal haemorrhage (n = 1), severe punctate WM lesions combined with parenchymal and extracerebral haemorrhage (n = 1), hypoxic-ischaemic encephalopathy (HIE; n = 1), and acute cerebral infarction (n = 1). The prevalence of additional MRI abnormalities was not significantly different between neonates with and without PVPCs in the study population in this period ($P > 0.05$, Table A1).

3.3. Microstructural alterations in different PVPC groups

The microstructural alterations were different between the 2 PVPC groups. No significant differences were found between group 1 and the control group ($P \geq 0.017$). In group 2, reduced FA, increased RD, and unchanged AD were observed in the genu and splenium of the corpus callosum, and posterior limbs of the internal capsule. In addition, reduced FA, increased RD, and increased AD were observed in multiple regions, including the anterior limbs of the internal capsule, corona radiate, superior longitudinal fasciculus, external capsule, posterior thalamic radiations, cerebral peduncle, inferior fronto-occipital fasciculus, uncinate fasciculus, precentral gyrus and postcentral gyrus (Fig. 2). The detailed DTI parameters of the affected brain regions in each group are shown in Fig. 3.

4. Discussion

This study examined the extent of WM microstructural variations in PVPC neonates with and without additional MRI abnormalities, using TBSS combined with ROI analysis which have previously been described as sensitive methods to characterise neonatal WM microstructure. Our study demonstrated that isolated PVPCs were not associated with WM alterations, but revealed extensive WM changes in neonates with PVPCs combined with additional MRI abnormalities, including intracranial haemorrhage, mild to severe punctate WM lesions, HIE, and acute cerebral infarction.

The incidence of PVPCs detected by MRI in our study population was 14.24%, which is higher than that reported by most previous studies [2,9] but lower than that in the study by Hagmann et al. (15%) [24]. The higher incidence we report may be due to the sensitivity of MRI for visualisation of brain injuries, especially smaller cysts that are easily missed by US. In addition, unlike routine screening with US, MRI is only used to diagnose lesions that either cannot or cannot reliably be recognised with US in high-risk infants [25]. The existence of inclusion bias in our study population may also be one of the reasons for the high incidence that we report.

4.1. Location of PVPCs

The PVPCs included in our study were mainly located at the CTN/adjacent to the head of the caudate nucleus, followed by the frontal and occipital horns of the lateral ventricles. This is in keeping with previous findings that the PVPC location has been suggested to indicate the likely period of their formation [2]. The germinal matrix at the CTN/adjacent to the head of the caudate nucleus is active until GA weeks 34–35; therefore, a PVPC in that location can occur anytime during this time window [2]. The regression of germinal matrix follows a posterior to anterior sequence during brain development [26], with a low likelihood that it will be affected in the occipital horns. Although the germinal matrix of the frontal horns is the last to disappear, its relatively small area may restrict to the potential for damage relative to the CTN/adjacent to the head of the caudate nucleus. In addition, most PVPCs in

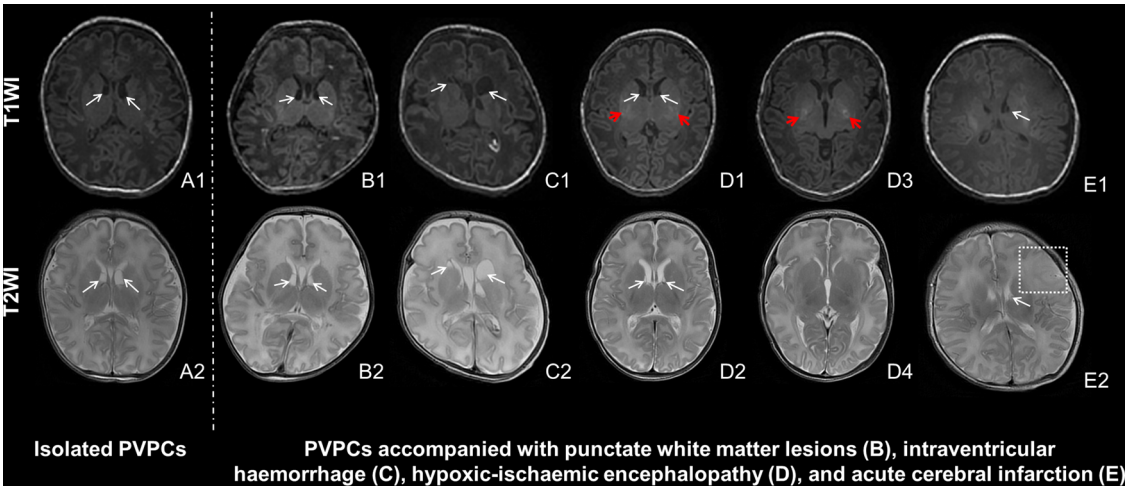

Fig. 1. Periventricular pseudocyst (PVPC) appearances on T1WI and T2WI.
(A) In a case with isolated PVPCs, the lesions are located in the bilateral caudothalamic notch (CTN)/adjacent to the head of the caudate nucleus (white arrows). (B–E) In 4 cases of PVPCs accompanied by severe punctate white matter lesions (B, hyperintense on T1WI and hypointense on T2WI), left intraventricular haemorrhage (C), hypoxic-ischaemic encephalopathy (D, red arrows) and acute cerebral infarction (E, white dotted square; hyperintense on DTI and hypointense on ADC map); the pseudocysts are located in the bilateral CTN/adjacent to the head of the caudate nucleus, bilateral frontal horns, bilateral CTN/adjacent to the head of the caudate nucleus, and left CTN/adjacent to the head of the caudate nucleus, respectively (white arrows).

our study population showed a left-side predilection. This observation is in accordance with those of previous studies showing that left-side laterality might be associated with poor blood circulation in the left hemisphere, which is influenced both by the inherent vascular anatomy of the foetus, and the preference of newborns for lying with their heads to the right [27]. In summary, the duration of the germinal matrix and cerebral blood flow together contribute to the distribution of PVPCs.

4.2. Microstructural alterations in different PVPC groups

During the neonatal period, proliferation of oligodendrocytes lineage precursors (pre-myelination stage, decreased RD and AD, and increased FA) and axonal myelination (myelination stage, decrease in RD and an increase in FA with no significant change in AD) are two main developmental processes could be observed through alterations in

Table 1
Perinatal characteristics[a] and clinical histories[a] of neonates with PVPCs[b] and controls.

	Group 1 (n = 15)	Group 2 (n = 23)	Control group (n = 60)	*P1*[c]	*P2*[d]
Sex (male/female)	10/5	10/13	40/20	1.00	0.05
GA[b](weeks)	39.57 (35.86–41.43)	39.14 (30.71–40.86)	39.21 (28.29–41.71)	0.25	0.34
Preterm/full-term ratio	1/14	6/17	11/49	0.43	0.48
Age at MRI (days)	10 (2–20)	10 (0–26)	11 (1–28)	0.22	0.51
BW[b](g)	3320 (2100–4200)	3030 (1670–4170)	3200 (1250–4800)	0.72	0.12
Head circumference (cm)	34 (32–36)	34 (28–35)	34 (30–52)	0.82	0.70
Body length (cm)	50 (46–53)	49 (43–52)	50 (36–55)	0.68	0.14
Mode of delivery (vaginal/caesarean)	9/6	13/10	24/34	0.20	0.22
Metabolic acidosis[e]	5 (33.33)	6 (26.09)	4 (6.67)	0.02	0.04
Mild asphyxia[f]	3 (20.00)	4 (17.39)	9 (15.00)	0.94	1.00
Pneumonia	2 (13.33)	5 (30.43)	21 (35.00)	0.24	0.24
Clinical Infection alone[g]	2 (6.67)	7 (30.43)	0 (0.00)	0.01	< 0.001
Rotavirus enteritis	0 (0.00)	2 (8.70)	4 (6.67)	0.70	1.00
Physiologic jaundice	6 (40.00)	6 (26.09)	9 (15.00)	0.07	0.39
Haemolysis	2 (13.33)	1 (4.35)	6 (10.00)	1.00	0.74
Congenital heart diseases[h]	0 (0.00)	5(21.74)	4 (6.67)	0.67	0.11
History of maternal hypertension[i]	0 (0.00)	0 (0.00)	2 (0.05)	1.00	1.00
History of maternal diabetes[j]	0 (0.00)	0 (0.00)	1 (0.02)	1.00	1.00
Positive for TORCH[b]screening	2 (13.33)	2 (8.70)	0 (0.00)	–	–

[a] Data are expressed as the median (range) or number (percentage).
[b] Abbreviations: PVPC, periventricular pseudocyst; BW, birth weight; GA, gestational age; TORCH, routine toxoplasmosis, rubella, cytomegalovirus, and herpes simplex virus.
[c] *P* value of Group 1 *vs.* Control group.
[d] *P* value of Group 2 *vs.* Control group.
[e] The median base excess of the newborns in Group 1, Group 2 and Control Group were −14.40 mmol/L (−8.10 mmol/L ~ −17.60 mmol/L), −12.30 mmol/L (−8.40 mmol/L ~ −29.2 mmol/L), and −8.30 mmol/L (−6.00 mmol/L ~ −9.30 mmol/L) respectively.
[f] Assessed by ICD-10 categories of the diagnosis "perinatal asphyxia" defined by clinical signs and 1-min APGAR score [40]; 1-min APGAR score of 4–7 was categorised as mild asphyxia; the median 1-min APGAR scores of the newborns in Group 1, Group 2 and Control Group were 7 (5–7), 6 (4–7) and 7 (5–7) respectively.
[g] The diagnosis "clinical infection alone" defined by late-onset (> 72 hours) cultures negative but antibiotic treatment for ≥5 days.
[h] Group 2 included 2 cases of ventricular septal defect, 2 cases of atrial septal defect with ventricular septal defect, and 1 case of atrial septal defect; Control Group included 3 cases of ventricular septal defect and 1case of patent ductus arteriosus.
[i] Both of the 2 cases were diagnosed with "gestational hypertension".
[j] The case was diagnosed with "gestational diabetes mellitus".

Table 2
MRI features of the two PVPC groups.

Imaging features	All groups (n = 38)	Group 1 (n = 15)	Group 2 (n = 23)	*P*
Lateralization (No.)				0.61
Bilateral	21 (55.26)	9 (60.00)	12 (52.17)	
Left	12 (31.58)	5 (33.33)	7 (30.43)	
Right	5 (13.16)	1 (6.67)	4 (17.39)	
Uni-/multilocular (No.)				1.00
Unilocular	34 (89.47)	14 (93.33)	20 (87.0)	
Multilocular	4 (10.53)	1 (6.67)	3 (13.04)	
Location (No.)				0.31
Frontal horns	5 (13.16)	1 (6.67)	4 (17.39)	
CTN/ adjacent to the head of caudate nucleus	33 (86.84)	15 (100)	18 (78.26)	
Temporal horns	0 (0)	0 (0)	0 (0)	
Occipital horns	1 (2.63)	0 (0)	1 (4.35)	
Anteroposterior diameter (mm)	5.97 (3.67-10.20)	5.89 (3.93–7.77)	6.26 (3.49–12.03)	0.40

Data are expressed as the number (percentage) or median (range).

DTI metrics [28,29]. TBSS has emerged as a general approach for investigating the development of major WM skeletons of whole brain, and ROI analysis further provides a complementary detailed impression into differential microstructural brain development between groups [14,15]. Our study revealed that isolated PVPCs did not cause changes in the WM, which is consistent with most previous studies that have shown that isolated PVPCs have a favourable prognosis [1,8,9]. Early autopsy study has proven that cells in the germinal matrix proliferate actively in early development [30]. Additionally, even oligodendrocyte progenitor cells can proliferate to compensate for cell loss when exposed risk factors [31]. Thus, the remaining cells of the germinal matrix and the radial cells may proliferate to compensate partially for the initial cell loss, contributing to the unchanged DTI parameters associated with isolated PVPCs. Furthermore, most of the PVPCs enrolled in our study were focal and unilocular, and such compensation allows the germinal matrix to continue to involute on schedule in later development. Most PVPCs mainly occur early in life, when the organisation of the networks of neuronal synapses as well as that of WM pathways is ongoing [32]. However, some studies have found that PVPCs are associated with abnormal development. These discrepancies might be due to biases in research design (i.e., case reports or series), the inclusion of infants with additional US abnormalities, or the enrolment of subjects without a normative control group [3,7,27]. As a whole, germinal matrix compensation mechanisms and high early-life plasticity may contribute to restoring the function of damaged cells in neonates with isolated PVPCs.

In neonates with PVPCs combined with additional cerebral injury, the reduced FA, increased RD, and increased/unchanged AD that characterise extensive WM alterations result from the pathologies of the accompanying injury. It is possible that the effect of a PVPC on WM microstructure might differ when it is accompanied by additional injuries, but a localised lesion with a favourable prognosis is unlikely to cause such widespread DTI changes. In contrast to the microhaemorrhage that causes PVPCs, more extensive of germinal matreix-intraventricular haemorrhage have a significant direct effect on

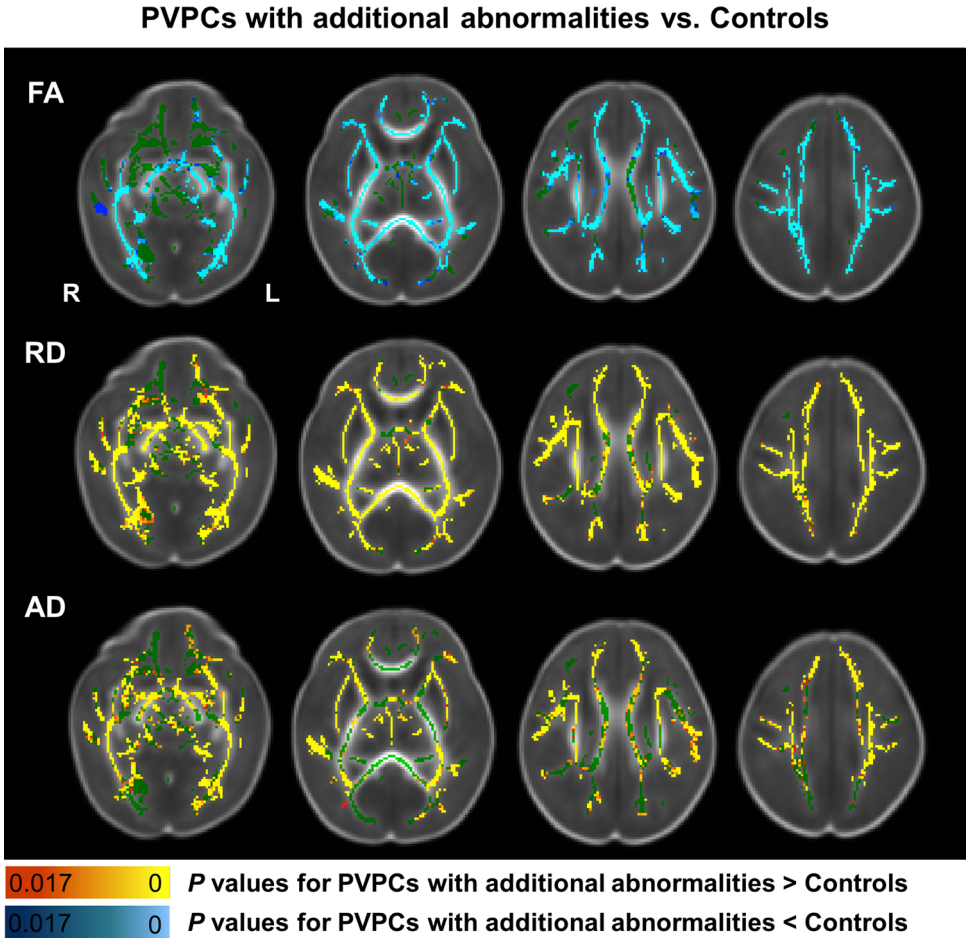

Fig. 2. Changes in fractional anisotropy (FA), radial diffusivity (RD), and axial diffusivity (AD) in neonates with periventricular pseudocysts (PVPCs) with additional abnormalities.

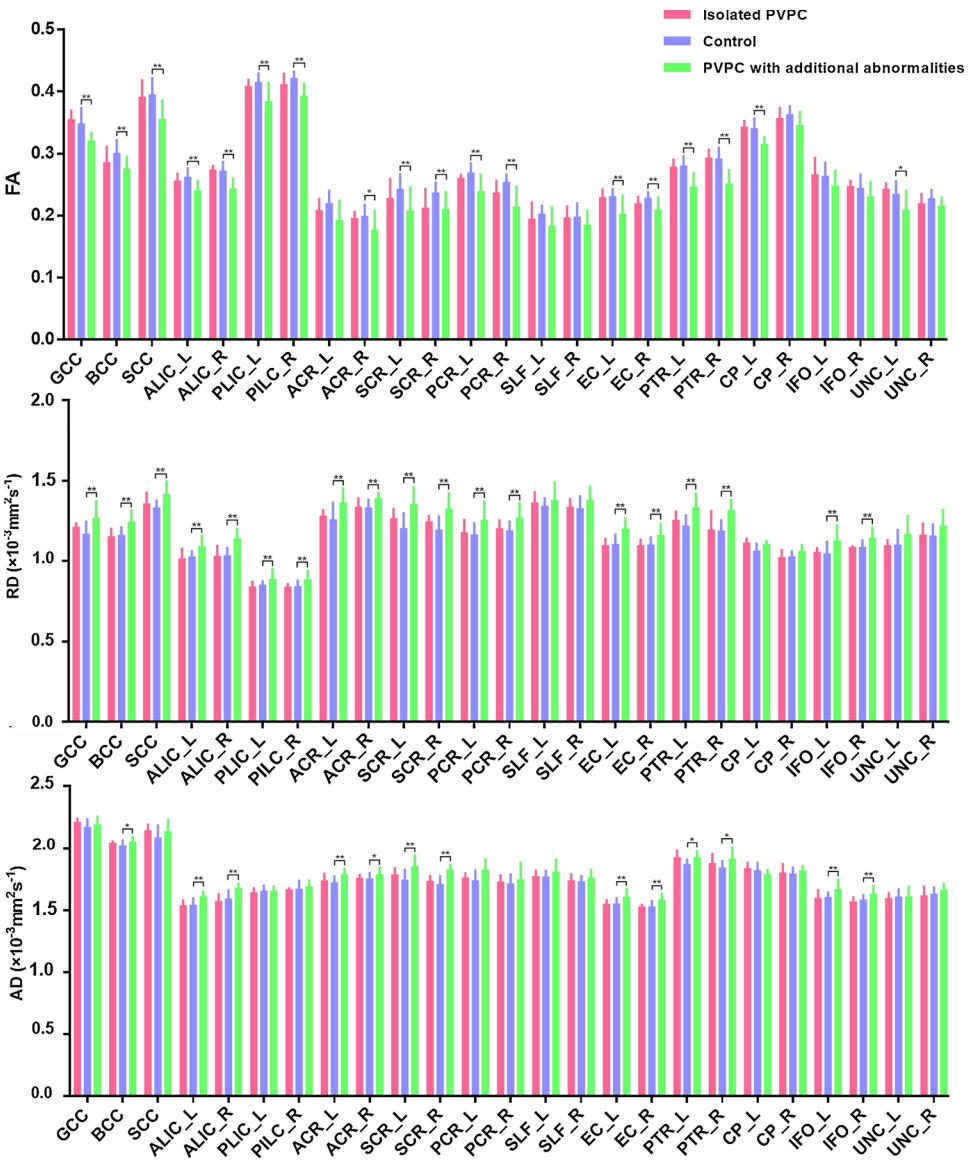

Fig. 3. Fractional anisotropy (FA), radial diffusivity (RD), and axial diffusivity (AD) values of different brain regions in neonates with periventricular pseudocysts (PVPCs; isolated or accompanied by additional abnormalities) and controls.
Imaging data are analysed using tract-based spatial statistics. GCC, genu of corpus callosum; BCC, body of corpus callosum; SCC, splenium of corpus callosum; ALIC, anterior limb of internal capsule; PLIC, posterior limb of internal capsule; ACR, anterior corona radiate; SCR, superior corona radiate; PCR, posterior corona radiate; SLF, superior longitudinal fasciculus; EC, external capsule; PTR, posterior thalamic radiation; CP, cerebral peduncle; IFO, inferior fronto-occipital fasciculus; UNC, uncinate fasciculus; L, left; R, right. All values are shown as the median and interquartile range. *, $P < 0.017$; **, $P < 0.001$.

oligodendroglia and astrocytes produced by germinal matrix, which are important for myelination [17,31]. Other types of haemorrhage may result in WM damage mainly through the increased concentrations of free radicals and inflammatory cytokines induced by microglial activation [17,33,34]. Due to punctate WM lesions, HIE and acute cerebral infarction usually involve multiple WM areas, making changes in DTI metrics more extensive and significant [17,35–37]. Significantly decreased FA, increased RD, and unchanged AD could reflect the effect of injuries on WM in myelination stage, including the genu and splenium of the corpus callosum and posterior limbs of the internal capsule [38,39]. This observation may be attributable to the dysfunction of immature oligodendrocytes, which are highly vulnerable to hypoxic-ischaemic injury [38]. Disrupted cross-talk between an axon and oligodendrocytes would delay the early process of oligodendrocyte proliferation or lead to the death of oligodendrocyte progenitors in pre-myelination stage [17]. Decrease in FA, and increases in RD and AD in extensive regions of WM may reveal this process. In general, our TBSS and ROI findings revealed the integrative effects of these accompanying injuries in group 2.

Our study has several limitations. Although the incidence rate (14.24%) of PVPCs in our study population is significantly higher than that in previous reports (0.5–5.8%) [1,3–5], our sample size in each group was still not large enough. In addition, grey matter development was not evaluated at the time of our study. Finally, the follow-up of these neonates is incomplete due to the retrospective analysis. Future studies would ideally enrol more subjects to further verify the relationship between early brain microstructural parameters and neurodevelopment outcomes.

5. Conclusion

Isolated PVPCs are not independently correlated with WM microstructural variations during brain development in neonates. Our results provide further evidence for supporting the benign outcome of fetuses with isolated PVPCs, which is vital for parental counselling and obstetric management.

6. Conflict of interest

The authors declare that they have no conflict of interest.

7. Funding acknowledgement

This work was supported by the grant from the National Key Research and Development Program of China (2016YFC0100300), National Natural Science Foundation of China (81771810, 81471631,

and 51706178), the 2011 New Century Excellent Talent Support Plan of the Ministry of Education, China (NCET-11-0438), the Clinical Research Award of the First Affiliated Hospital of Xi'an Jiaotong University (XJTU1AF-CRF-2015-004), the Fundamental Research Funds for the Central Universities (xjj2018265), and the Youth Innovation Fund of the First Affiliated Hospital of Xi'an Jiaotong University (2017QN-09).

8. Informed consent

Informed consent was obtained from the guardians of all individual participants included in this study.

Acknowledgements

We thank all the families who participated in the study.

Appendix A

Table A1
Additional MRI abnormalities between neonates with and without PVPCs.

Additional MRI abnormalities	Neonates with PVPCs (n = 46)	Neonates without PVPCs (n = 277)	*P*
Extracerebral haemorrhage	13 (28.26)	62 (22.38)	0.36
Parenchymal haemorrhage	7 (15.22)	19 (6.86)	0.10
Intraventricular haemorrhage	4 (8.70)	16 (5.78)	0.67
Punctate WM lesions	13(28.26)	87 (31.41)	0.67
Hypoxic-ischaemic encephalopathy	1 (2.17)	6 (2.17)	1.00
Acute cerebral infarction	1 (2.17)	5 (1.81)	1.00
Congenital malformation	1 (2.17)	2 (0.72)	0.90
Hydrocephalus	–	3 (1.08)	–
Hypoglycemia encephalopathy	–	4 (1.44)	–
Periventricular leukomalacia	–	2 (0.72)	–
Basal ganglia abnormalities	–	3 (1.08)	–

Data are expressed as the number (percentage), – means not applicable.

References

[1] F. Wong, S. Fraser, E. Kelly, C. Acton, Clinical significance of isolated paraventricular cysts on cranial ultrasonography, J. Paediatr. Child Health 40 (2004) 552–555, https://doi.org/10.1111/j.1440-1754.2004.00462.x.
[2] M.A. Zoppi, A. Iuculano, M.T. Peltz, G. Monni, Prenatal detection of periventricular pseudocysts by ultrasound: diagnosis and outcome, Case Rep. Perinat. Med. 1 (2012) 75–78, https://doi.org/10.1515/crpm-2012-0008.
[3] H. Esteban, E. Blondiaux, E. Audureau, C. Sileo, M.L. Moutard, A. Gelot, et al., Prenatal features of isolated subependymal pseudocysts associated with adverse pregnancy outcome, Ultrasound Obstet. Gynecol. 46 (2015) 678–687, https://doi.org/10.1002/uog.14820.
[4] Y.C. Chuang, C. Lee, N.C. Chiu, C.H. Shu, H.Y. Hung, H.A. Kao, et al., Neurodevelopment in very low birth weight premature infants with postnatal subependymal cysts, J. Child Neurol. 22 (2007) 402–405, https://doi.org/10.1177/0883073807301924.
[5] K.J. Rademaker, L.S. De Vries, P.G. Barth, Subependymal pseudocysts: ultrasound diagnosis and findings at follow-up, Acta Paediatr. 82 (1993) 394–399, https://doi.org/10.1111/j.1651-2227.1993.tb12705.x.
[6] L. Thun-Hohenstein, I. Forster, C. Kunzle, E. Martin, E. Boltshauser, Transient bifrontal solitary periventricular cysts in term neonates, Neuroradiology 36 (1994) 241–244, https://doi.org/10.1007/bf00588143.
[7] C. Zorzi, I. Angonese, Subependymal pseudocysts in the neonate, Eur. J. Pediatr. 148 (1989) 462–464, https://doi.org/10.1007/bf00595915.
[8] S. Unger, S. Salem, L. Wylie, V. Shah, Newborn frontal horn cysts: cause for concern? J. Perinatol. 31 (2011) 98–103, https://doi.org/10.1038/jp.2010.79.
[9] H. Chang, C.M. Tsai, C.Y. Hou, S.H. Tseng, J.C. Lee, M.L. Tsai, Multiple subependymal pseudocysts in neonates play a role in later attention deficit hyperactivity and autistic spectrum disorder, J. Formos. Med. Assoc. 118 (2019) 692–699, https://doi.org/10.1016/j.jfma.2018.08.007.
[10] S. Cooper, O. Bar-Yosef, Prenatal evaluation, imaging features, and neurodevelopmental outcome of prenatally diagnosed periventricular pseudocysts, AJNR Am. J. Neuroradiol. 37 (2016) 2382–2388, https://doi.org/10.3174/ajnr.a4916.
[11] C. Raybaud, T. Ahmad, N. Rastegar, M. Shroff, M. Al Nassar, The premature brain: developmental and lesional anatomy, Neuroradiology 55 (Suppl 2) (2013) 23–40, https://doi.org/10.1007/s00234-013-1231-0.
[12] K. Schadl, R. Vassar, K. Cahill-Rowley, K.W. Yeom, D.K. Stevenson, J. Rose, Prediction of cognitive and motor development in preterm children using exhaustive feature selection and cross-validation of near-term white matter microstructure, NeuroImage Clinical. 17 (2018) 667–679, https://doi.org/10.1016/j.nicl.2017.11.023.
[13] P. Krishnan, P. Muthusami, C. Heyn, M. Shroff, Advances in pediatric neuroimaging, Indian J. Pediatr. 82 (2015) 154–165, https://doi.org/10.1007/s12098-014-1657-3.
[14] X. Li, J. Gao, M. Wang, M. Wan, J. Yang, Rapid and reliable tract-based spatial statistics pipeline for diffusion tensor imaging in the neonatal brain: applications to the white matter development and lesions, Magn. Reson Imaging. 34 (2016) 1314–1321, https://doi.org/10.1016/j.mri.2016.07.011.
[15] H.M. Feldman, J.D. Yeatman, E.S. Lee, L.H. Barde, S. Gaman-Bean, Diffusion tensor imaging: a review for pediatric researchers and clinicians, J. Dev. Behav. Pediatr. 31 (2010) 346–356, https://doi.org/10.1097/DBP.0b013e3181dcaa8b.
[16] X. Li, J. Gao, M. Wang, J. Zheng, Y. Li, E.S. Hui, et al., Characterization of extensive microstructural variations associated with punctate White matter lesions in preterm neonates, AJNR Am. J. Neuroradiol. 38 (2017) 1228–1234, https://doi.org/10.3174/ajnr.A5226.
[17] D. Tortora, C. Martinetti, M. Severino, S. Uccella, M. Malova, A. Parodi, et al., The effects of mild germinal matrix-intraventricular haemorrhage on the developmental white matter microstructure of preterm neonates: a DTI study, Eur. Radiol. 28 (2017) 1157–1166, https://doi.org/10.1007/s00330-017-5060-0.
[18] A. Vade, R. Sukhani, M. Dolenga, C. Habisohn-Schuck, Chloral hydrate sedation of children undergoing CT and MR imaging: safety as judged by American academy of pediatrics guidelines, AJR Am. J. Roentgenol. 165 (1995) 905–909, https://doi.org/10.2214/ajr.165.4.7676990.
[19] J.P. Cravero, G.T. Blike, M. Beach, S.M. Gallagher, J.H. Hertzog, J.E. Havidich, et al., Incidence and nature of adverse events during pediatric sedation/anesthesia for procedures outside the operating room: report from the pediatric sedation research consortium, Pediatrics 118 (2006) 1087–1096, https://doi.org/10.1542/peds.2006-0313.
[20] M. Epelman, A. Daneman, S.I. Blaser, C. Ortiz-Neira, O. Konen, J. Jarrin, O.M. Navarro, Differential diagnosis of intracranial cystic lesions at head US: correlation with CT and MR imaging, Radiographics 26 (2006) 173–196, https://doi.org/10.1148/rg.261055033.
[21] S.M. Smith, M. Jenkinson, M.W. Woolrich, C.F. Beckmann, T.E. Behrens, H. Johansen-Berg, et al., Advances in functional and structural MR image analysis and implementation as FSL, NeuroImage 23 (2004) S208–219, https://doi.org/10.1016/j.neuroimage.2004.07.051.
[22] X. Li, J. Yang, J. Gao, X. Luo, Z. Zhou, Y. Hu, et al., A robust post-processing workflow for datasets with motion artifacts in diffusion kurtosis imaging, PloS One 9 (2014) e94592, https://doi.org/10.1371/journal.pone.0094592.
[23] K. Oishi, S. Mori, P.K. Donohue, T. Ernst, L. Anderson, S. Buchthal, et al., Multi-contrast human neonatal brain atlas: application to normal neonate development analysis, NeuroImage 56 (8-2) (2011), https://doi.org/10.1016/ j.neuroimage.2011.01.051.
[24] C.F. Hagmann, N.J. Robertson, D. Acolet, D. Chan, S. Onda, N. Nyombi, et al., Cranial ultrasound findings in well newborn Ugandan infants, Arch. Dis. Child Fetal. 95 (2010) 338–344, https://doi.org/10.1136/adc.2009.174607.
[25] L.S. de Vries, M.J. Benders, F. Groenendaal, Imaging the premature brain: ultrasound or MRI? Neuroradiology 55 (Suppl 2) (2013) 13–22, https://doi.org/10.1007/s00234-013-1233-y.

[26] M. Battin, E.F. Maalouf, S. Counsell, A.H. Herilhy, A.D. Edwards, Magnetic resonance imaging of the brain of premature infants, Lancet 349 (1997) 1741, https://doi.org/10.1016/s0140-6736(97)24024-9.
[27] E. Herini, S. Tsuneishi, S. Takada, Sunarini, H. Nakamura, Clinical features of infants with subependymal germinolysis and choroid plexus cysts, Pediatr. Int. 45 (2003) 692–696, https://doi.org/10.1046/j.1442-200x.2003.01814.x.
[28] J. Dubois, G. Dehaene-Lambertz, M. Perrin, J.F. Mangin, Y. Cointepas, E. Duchesnay, et al., Asynchrony of the early maturation of white matter bundles in healthy infants: quantitative landmarks revealed noninvasively by diffusion tensor imaging, Human brain mapping 29 (2008) 14–27, https://doi.org/10.1002/hbm.20363.
[29] J. Dubois, G. Dehaene-Lambertz, S. Kulikova, C. Poupon, P.S. Huppi, L. Hertz-Pannier, The early development of brain white matter: a review of imaging studies in fetuses, newborns and infants, Neuroscience 276 (2014) 48–71, https://doi.org/10.1016/j.neuroscience.2013.12.044.
[30] A. Simonati, C. Tosati, T. Rosso, E. Piazzola, N. Rizzuto, Cell proliferation and death: morphological evidence during corticogenesis in the developing human brain, Microsc. Res. Tech. 45 (1999) 341–352, https://doi.org/10.1002/(sici)1097-0029(19990615)45:6<341::aid-jemt2>3.0.co;2-u.
[31] A. Barateiro, V.E. Miron, S.D. Santos, J.B. Relvas, A. Fernandes, C. Ffrench-Constant, et al., Unconjugated bilirubin restricts oligodendrocyte differentiation and axonal myelination, Mol. Neurobiol. 47 (2013) 632–644, https://doi.org/10.1007/s12035-012-8364-8.
[32] M.V. Johnston, A. Ishida, W.N. Ishida, H.B. Matsushita, A. Nishimura, M. Tsuji, Plasticity and injury in the developing brain, Brain Dev. 31 (2009) 1–10, https://doi.org/10.1016/j.braindev.2008.03.014.
[33] X. Ou, C.M. Glasier, R.H. Ramakrishnaiah, S.B. Mulkey, Z. Ding, T.L. Angtuaco, et al., Impaired white matter development in extremely low-birth-weight infants with previous brain hemorrhage, AJNR Am. J. Neuroradiol. 35 (2014) 1983–1989, https://doi.org/10.3174/ajnr.A3988.
[34] V. Supramaniam, R. Vontell, L. Srinivasan, J. Wyatt-Ashmead, H. Hagberg, M. Rutherford, Microglia activation in the extremely preterm human brain, Pediatr. Res. 73 (2013) 301–309, https://doi.org/10.1038/pr.2012.186.
[35] L. Bassi, A. Chew, N. Merchant, G. Ball, L. Ramenghi, J. Boardman, J.M. Allsop, et al., Diffusion tensor imaging in preterm infants with punctate white matter lesions, Pediatr. Res. 69 (2011) 561–566, https://doi.org/10.1203/PDR.0b013e3182182836.
[36] O. Brissaud, M. Amirault, F. Villega, O. Periot, J.F. Chateil, M. Allard, Efficiency of fractional anisotropy and apparent diffusion coefficient on diffusion tensor imaging in prognosis of neonates with hypoxic-ischemic encephalopathy: a methodologic prospective pilot study, AJNR Am. J. Neuroradiol. 31 (2010) 282–287, https://doi.org/10.3174/ajnr.A1805.
[37] N.E. van der Aa, F.J. Northington, B.S. Stone, F. Groenendaal, M.J. Benders, G. Porro, et al., Quantification of white matter injury following neonatal stroke with serial DTI, Pediatr. Res. 73 (2013) 756–762, https://doi.org/10.1038/pr.2013.45.
[38] S. Wang, E.X. Wu, C.N. Tam, H.F. Lau, P.T. Cheung, P.L. Khong, Characterization of white matter injury in a hypoxic-ischemic neonatal rat model by diffusion tensor MRI, Stroke 39 (2008) 2348–2353, https://doi.org/10.1161/strokeaha.107.509927.
[39] M. Ouyang, J. Dubois, Q. Yu, P. Mukherjee, H. Huang, Delineation of early brain development from fetuses to infants with diffusion MRI and beyond, NeuroImage 185 (2018) 836–850, https://doi.org/10.1016/j.neuroimage.2018.04.017.
[40] Basis Newborn Resuscitation: a Practical Guide, World Health Organisation, 1998 http://apps.who.int/iris/bitstream/10665/63953/1/WHO_RHT_MSM_98.1.pdf Accessed 6 April, 2019.